Supporting Information

Growth Mode Transition from Monolayer by Monolayer to Bilayer by Bilayer in Molecularly Flat Titanyl Phthalocyanine Film

Jun Hong Park,[†] Lalitasri Ravavar,[#] Iljo Kwak,[†] Susan K. Fullerton-Shirey,[‖] Pabitra Choudhury,[#] Andrew C. Kummel[†,‡]*

[†]Materials Science & Engineering Program, University of California, San Diego, La Jolla, CA, 92093, U.S.A.

[‡]Departments of Chemistry & Biochemistry, University of California, San Diego, La Jolla, CA, 92093, U.S.A.

[#]Department of Chemical Engineering, New Mexico Tech, Socorro, NM 87801, U.S.A.

[‖]Department of Chemical and Petroleum Engineering, University of Pittsburgh, Pittsburgh, PA, 15213, U.S.A.

1. Bilayer and multilayer growth behavior of CuPc molecules on Au(111).

To compare the growth behavior of TiOPc molecules with the growth of planar metal phthalocyanines, monolayers ("ML") and bilayers ("BL") of CuPc are grown on Au(111). Fig. S1(a) shows the molecular structure of CuPc. Similar to TiOPc molecules, four aromatic benzene rings surround the central metal atom and N atoms.[1-2] However, at the center of the CuPc, there is only the Cu atom, resulting in a planar structure. Therefore, there is no difference in STM observations between face up and down in the CuPc layer.

To deposit ML CuPc, thick overlayers are deposited on Au(111); afterwards, the CuPc/Au(111) sample is annealed at 573 K for 4 mins. For the ML CuPc deposited on Au(111), the herringbone pattern of Au(111) is displayed through the CuPc ML (Fig. S1(b)). As shown in the molecularly resolved STM image of Fig S1(c), four-fold symmetric ML CuPc is observed, consistent with a previously reported result from Lu *et al*.[1] Unlike TiOPc molecules, the centers of the CuPc molecules are observed as dark holes because the d-orbital of the Cu atom in the CuPc molecule does not contribute to the tunneling process.[1-2] The band structure of the center CuPc is shown by scanning tunneling spectroscopy (STS), Fig. S1(d). The band gap is about 1.51 eV and the Fermi level of the Cu atom in CuPc is positioned in the near middle of band gap.

The additional deposition of CuPc molecules on the CuPc ML at 373 K results in BL and third layer (TL) growth, consistent with previous results by Takada *et al.*[3] In Fig. S1(e), a large size BL island is observed on the CuPc ML. While the growth of TiOPc BLs is initiated from multiple adsorption sites to form coherent crystalline islands on the TiOPc ML, the growth of the CuPc BL is initiated by the diffusion of newly absorbed CuPc molecules to the edge of a single island on CuPc MLs. Moreover, the growth of the CuPc TL is initiated on the CuPc BL, even

though the filling of the CuPc BL on the CuPc ML is not completed. As shown in the expanded STM image of Fig. S1(f), the CuPc TL is observed on the CuPc BL without completion of BL growth, similar to previous STM observations reported by Takada *et al* on CuPc/Au(111)[3-4]. Even the CuPc forth layer (4-L) starts to grow on the CuPc TL before completion of the CuPc BL. Conversely, the growth of TiOPc TL is not initiated on the TiOPc BL, unless the TiOPc BL is nearly completely filled by TiOPc molecules. As shown by the yellow dash lines and arrows in Fig. S1(f), the growth of the CuPc TL is initiated at the step edge of the CuPc BL, and the growth of the CuPc 4-L also is initiated at the step edge of the CuPc TL, consistent with step flowing mode, which can be observed in the growth of other organic molecules.[5-7]

In order to elucidate the adsorption configuration of CuPc molecules in the BL, a molecularly resolved STM image is shown in Fig. S1(g). The CuPc molecules in the BL are placed exactly on top of the CuPc molecules in the ML, in contrast to TiOPc molecules in the BL. This adsorption configuration of CuPc molecules in Fig. S1(h) is consistent with previous STM imaging of the CoPc BL and the CoPc ML on Au(111) by Takada *et al.*[3]

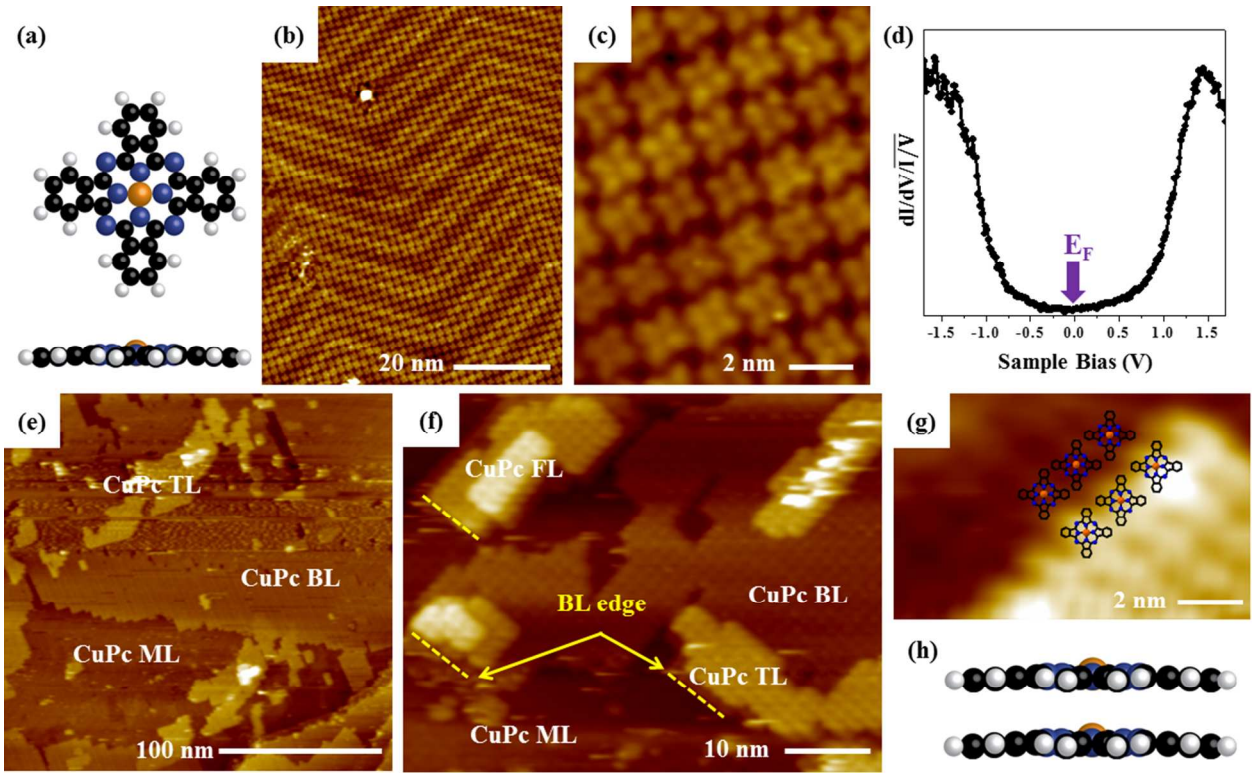

Figure S1. Deposition of MLs and BLs of CuPc on Au(111). (Vs = +2.0 V, It = 20 pA). (a) Molecular structure of CuPc. The center of the CuPc is assigned to the Cu atom shown as an orange sphere. The bottom schematic shows the planar structure of the CuPc molecule in contrast to the non-planar TiOPc. (b) Deposited ML CuPc on Au(111); the herringbone structure of Au(111) appears through the CuPc ML. (c) Expanded, filled-state STM image of ML CuPc. The center Cu atoms of CuPc are observed as dark holes. (d) STS taken at the center of the CuPc molecule; the Fermi level is in middle of band gap. (e) BL and third layer growth on CuPc ML at 373 K. (f) Expanded, empty state STM image of BL and TL growth on Au(111). (g) Molecularly resolved STM image at the edge of BL CuPc. (h) Stacking configuration of BL CuPc.

2. Multilayer growth behavior of CuPc molecules on Au(111).

To grow multilayers of CuPc on Au(111), additional CuPc is deposited on the CuPc ML at 373 K, consistent with about 3 nm thickness. As shown in Fig. S2(a), a polycrystalline CuPc top most surface is observed in STM, in contrast to a TiOPc multilayer with equivalent thickness. In the expanded STM image of Fig. S2(b), the heterogeneous stacking configuration of CuPc molecules appears, consist with two different stacking configurations; the flat stacking configuration dominates in CuPc multilayers, similar to BL, TL and 4-L of CuPc. However, some of the domains possess a tilted stacking of CuPc molecules, which is not observed in BL, TL and 4-L of CuPc. It can be hypothesized that as substrate-molecular interaction become weaker by pre-deposited CuPc layers, molecular-molecular interaction between CuPc molecules governs the growth behavior of the CuPc multilayer; therefore, the polymorphs of the crystal structure in the CuPc multilayers are generated by tilted stacking, consistent with a polycrystalline film.[8-9] The yellow box in Fig. S2(b) highlights the mixed stacking of tilted and flat CuPc molecules.

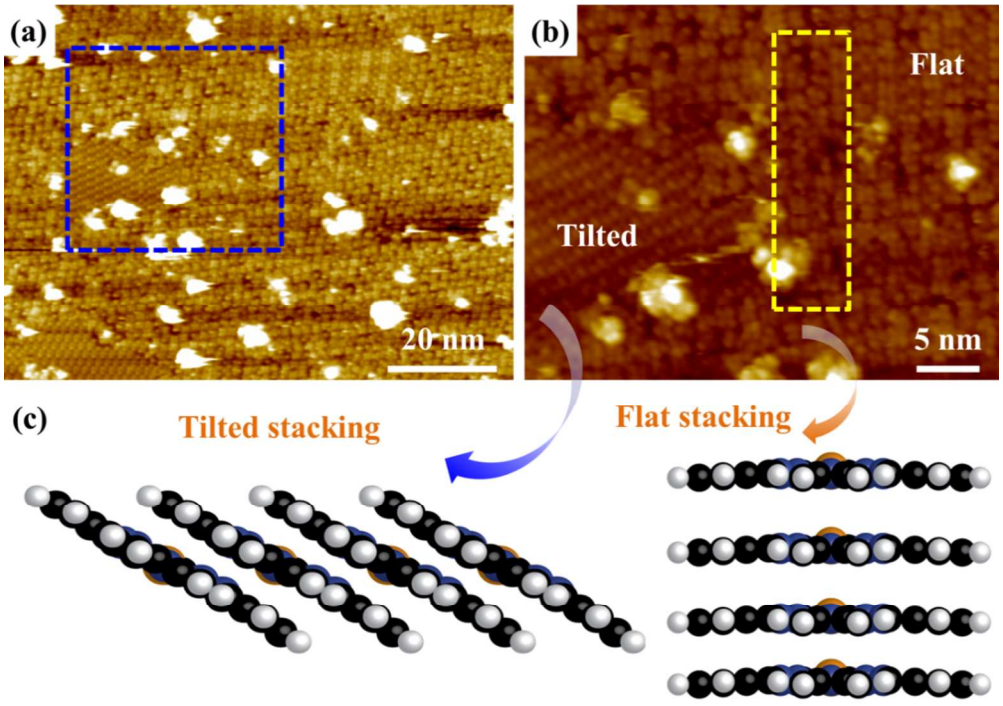

Figure S2. Deposition of Multilayer of CuPc on Au(111). (a) Large area empty state STM image. (Vs = +2.0 V, It = 20 pA). (b) Expanded STM image from the blue box in (a). (Vs = +1.2 V, It = 40 pA). Two different CuPc stackings can be observed. Yellow box displays local disordering. (c) Schematic shows tilted stacking and flat stacking configurations.

3. Bilayer growth of CuPc molecules on HOPG

The growth of CuPc BL on HOPG is similar growth to the growth of CuPc BL on Au(111). In Fig. S3(a), a CuPc ML is deposited on the HOPG surface with an identical growth method to CuPc ML on Au(111), forming four-fold, symmetric, molecular packing; the thick layer of CuPc molecules are deposited on the HOPG at 373 K, afterwards CuPc/HOPG sample is annealed at 573 K . In the expanded STM image of Fig. S3(b), partial desorption of CuPc molecules from the HOPG surface can be observed as shown by a white circle, resulting from post annealing at 573 K. Although both the CuPc ML on Au(111) and the CuPc ML on HOPG are annealed at 573 K for 4 mins during deposition of the MLs, desorption of CuPc molecules occurs only on HOPG, consistent the weaker interaction of CuPc-HOPG than the interaction of CuPc Au(111).

Similar electronic structures for CuPc ML/HOPG and CuPc ML/Au(111) are observed in STS. As shown by STS in Fig. S3(c), the band gap is about 1.57 eV and the Fermi level is positioned in the middle of band gap.

The additional deposition of CuPc molecules on CuPc ML/HOPG at 373 K results in the BL with similar growth behavior to CuPc/Au(111). In Fig. S3(d), a large size BL island is grown on CuPc ML/HOPG, even though CuPc ML is not filled fully.

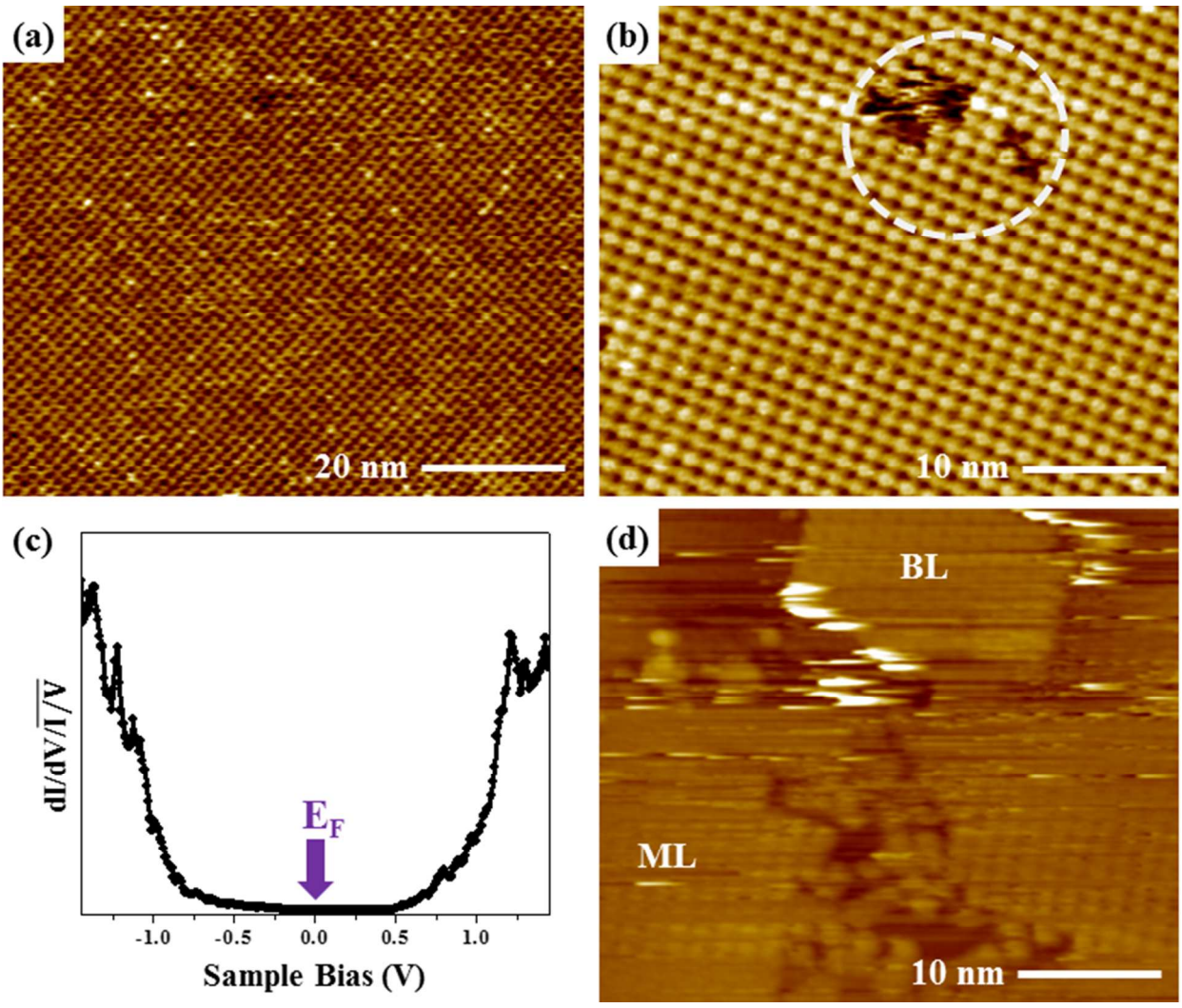

Figure S3. Deposition of ML and BL of CuPc on HOPG. (Vs = +2.0 V, It = 20 pA). (a) ML CuPc on HOPG deposited at 373 K. (b) Expanded empty state STM image of ML CuPc. A region of missing CuPc molecules is indicated by the white circle. (c) STS of CuPc/HOPG. The Fermi level is positioned at the center of band gap. (d) Empty state STM of BL CuPc growth on HOPG.

4. Estimation of thickness of deposited TiOPc layer using STM image

The growth rate and thickness of deposited films were estimated by investigation of pinholes in the TiOPc layers deposited for 1 min, as shown in Fig. S4. The rectangular shaped pinhole is observed in the nearly completed filled TiOPc layer. Through this pinhole two step edges are displayed; first step edge has about 3.2 Å height (green mark), and second step edge has about 2.5 Å height (red mark). The top layer has 6.1 Å height (blue mark), consistent with the formation of bilayer. Assuming the very bottom (yellow mark) is HOPG surface, the total number of deposited layer is at least 4 ML for 1 min. Since the height of benzene ring in typical MPc (metal Phthalocyanine) is about 2.5 – 3.0 Å[1-2], the estimated thickness of this layer is about 1.0 – 1.2 nm.

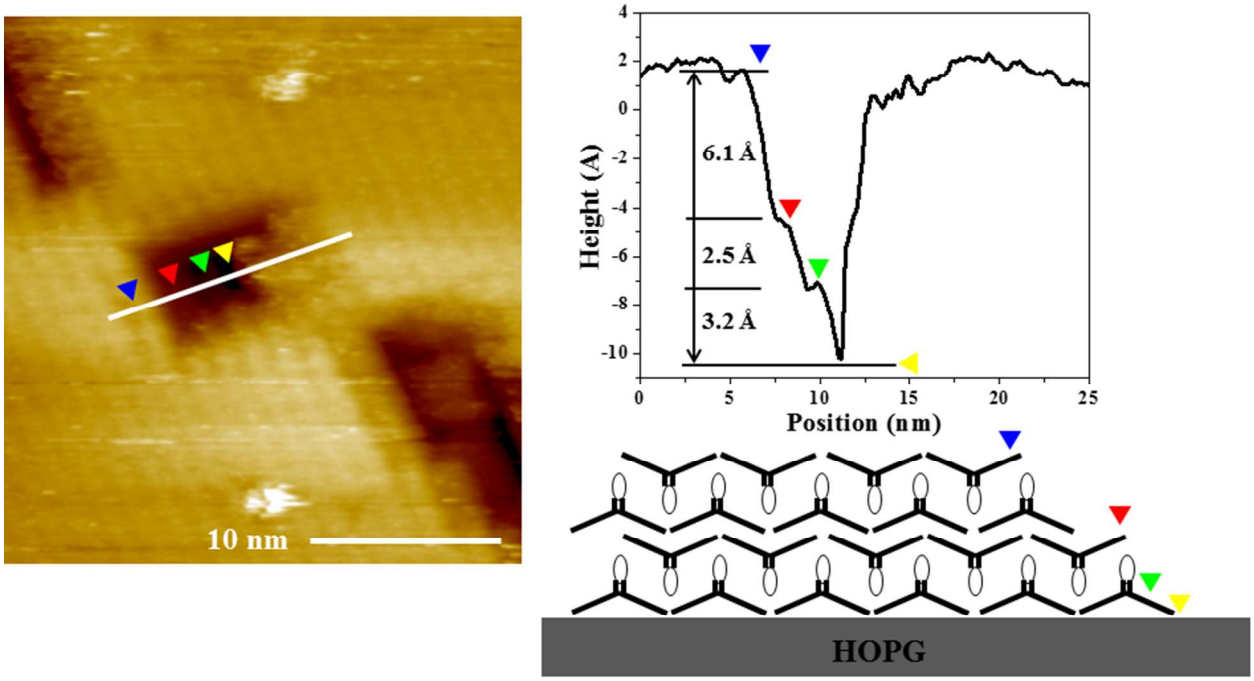

Figure S4. Estimation of TiOPc layer thickness in the STM image. The large pinhole is observed in TiOPc layer deposited for 1 min, as shown in STM image. About step edges of four TiOPc ML are detected through the pinhole, consistent with 4 ML/min. Therefore, the estimated thickness of this TiOPc layer (deposited for 1 min) are 1 – 1.2 nm following the 2.5 - 3.0 Å thickness of benzene ring.

5. Filling process of TiOPc during growth.

During the growth of TiOPc thin multilayers, back-to-back pairing of TiOPc molecules is initiated, after nearly completion of face-to-face pair pairing. In the TiOPc multilayer (about 2 nm), different coverage of face down oriented layers can be observed; the coverage is sorted from lower to higher in Fig. S4, consistent with the filling process of the face-down oriented layer. In Fig. S5(a), a few face-down oriented molecules adsorbed on the face-up oriented layer, and are dispersed uniformly. The region in the white box is expanded as an inset; the bright protrusion can be observed at the center of every molecule, consistent with the face-up orientation.

Figure S5(b) displays the intermediate coverage of the face-down oriented layer. If additional TiOPc molecules are adsorbed on the face-up oriented layer, a nearly full-coverage, face-down oriented layer is formed, as shown in Fig. S5(c). As shown by the white arrows, a few face-up oriented TiOPc molecules start to adsorb on the face-down oriented layer. Therefore, it can be concluded that during the growth of thin TiOPc multilayers, the formation of the face-up oriented layer is initiated, after near completion of face-down oriented layer filling.

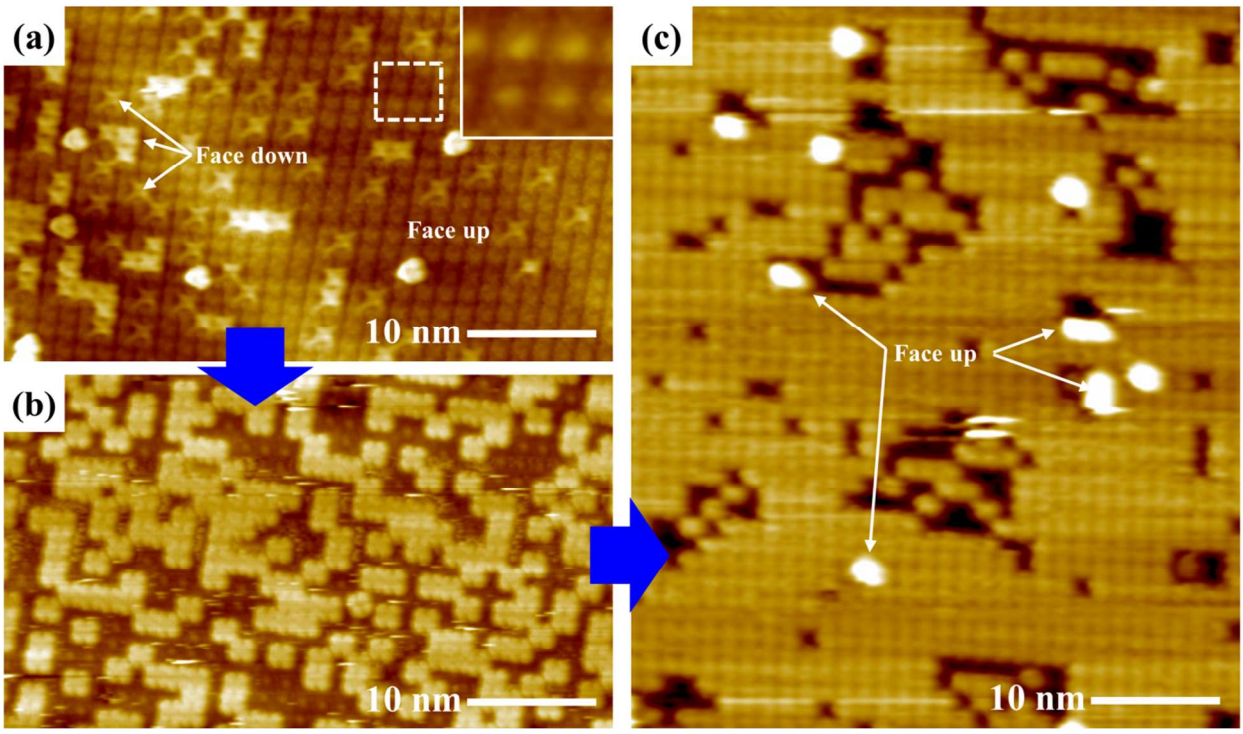

Figure S5. Filling process of TiOPc thin multilayer (about 2 nm) at 373 K. (Vs = +2.0 V, It = 20 pA). (a) Initial adsorption of face-down oriented molecules on a face-up oriented TiOPc layer. Insert shows the expanded image of white box. (b) Additional adsorption of face down oriented molecules. (c) Near fully filled, face-down oriented layer. The next face-up oriented molecules start to adsorb on the face-down oriented layer, as shown by the white arrows.

6. Large area STM image (250 nm x 250 nm) of thin TiOPc layer (about 2 nm)

Although both partially filled coverage and nearly fully filled coverage coexist in the single TiOPc layer, both areas have identical orientation, consistent with formation of large domains. As shown in the large area STM image in Fig. S6(a) 250 nm x 250 nm), two areas which have different coverage are observed. In the expanded STM image in Fig. S6(b), both the partially filled area and the nearly fully filled area have identical orientation. It can be hypothesized that stacking of sequent face up and down oriented TiOPc layer occurs coherently; consequently, even though there is coexistence of different coverage in a TiOPc layer, domain boundaries are not observed in 250 nm x 250 nm, consistent with the growth of large domains. It is noted that a few topmost TiOPc molecules are displayed as white spots in Fig. S6(b). The isolated molecularly adsorbed TiOPc molecules readily diffuse because of the absence of locking within close pack structures; therefore, the orientation of each TiOPc molecule cannot be estimated. Conversely, as shown by the yellow arrows, the clustered TiOPc molecules form a row and are aligned to substrate row of TiOPc, consistent with nearly identical orientation with the substrate layer.

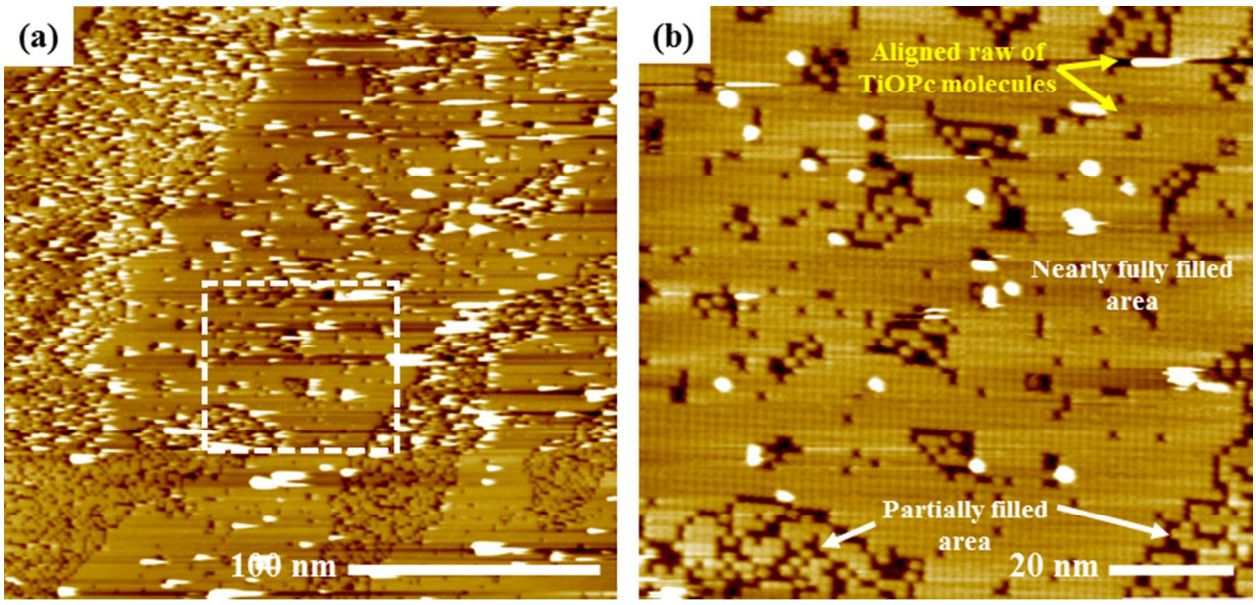

Figure S6. Large area STM image of TiOPc thin multilayer (about 2 nm). (Vs = +2.0 V, It = 20 pA). (a) 250 nm x 250 nm size STM image shown about 2 nm thick TiOPc layer. (b) Expanded STM image from white box in (a) shown both nearly fully filled area and partially filled area.

7. STS of TiOPc molecules in the multilayer (about 5 nm thickness)

In the multilayer of TiOPc, the Fermi level closer to the LUMO is still observed in STS, consistent with pervious TiOPc transistors fabricated in ultrahigh vacuum[10]. As shown by the STS of Fig. S7, the HOMO onset is located at -1.44 ± 0.01 V, while the LUMO onset is obtained at 1.04 ± 0.01 V, consistent with a 2.44 ± 0.02 eV band gap. Comparing the onset bias of HOMO and LUMO, the Fermi level is at 0.4 ± 0.02 V, closer to the LUMO than the HOMO, although the Fermi level is still located in the band gap.

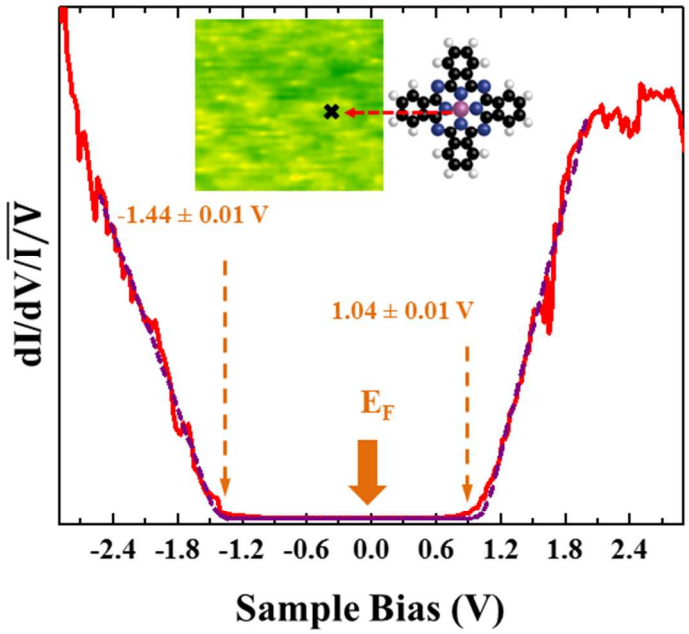

Figure S7. STS obtained on the center of TiOPc molecule in the BL and multilayer (about 5 nm thickness). The location of STS is marked as "X" in the superimposed STM image.

8. Suppressing the growth-mode transition of TiOPc from ML-by-ML to BL-by-BL at lower temperature, 343 K

The growth-mode transition from monolayer by monolayer (ML-by-ML) to bilayer by bilayer (BL-to-BL) can be suppressed by decreasing the deposition temperature. As shown in Fig. S8, multilayers of TiOPc are grown on HOPG at 343 K; the ML-by-ML growth mode can be observed in an STM image and a line trace of Fig. S8(a). After deposition of the TiOPc for an additional 3 mins on the multilayer of (a) at 343 K (estimated thickness: 5 nm), the ML-by-ML growth behavior still persists in Fig. S8(b). Conversely, the deposition of TiOPc multilayers at 373 K results in a growth-mode transition from ML-by-ML to BL-by-BL in TiOPc multilayers

deposited for equivalent times. Because the growth mode transition from ML-by-ML to BL-by-BL results from activating diffusion of face-up TiOPc molecules on a face-down TiOPc layer, it can be hypothesized that diffusion of TiOPc molecules is suppressed by the decreased deposition temperature.[11] However, even at the lower 373K temperature, additional deposition of multilayers to 10 nm thickness induced a transition in the growth mode to BL-by-BL as shown in Fig. S8(c), a large single BL is formed at the top most surface, consistent with about 0.6 nm height. Therefore, even for the lower deposition temperature, as the TiOPc film reaches a thickness that is sufficient to screen substrate-molecular interactions with pre-deposited TiOPc molecules, BL growth is observed for thick multilayer growth. It is noted that phthalocyanine has very high thermal stability, and decomposition only occurs above 923 K.[12] Therefore at 300 – 373 K, temperature range employed during deposition, the decomposition of TiOPc can be ruled out; however, the TiOPc molecule might be able to flip from face up to face down through a rotational motion.

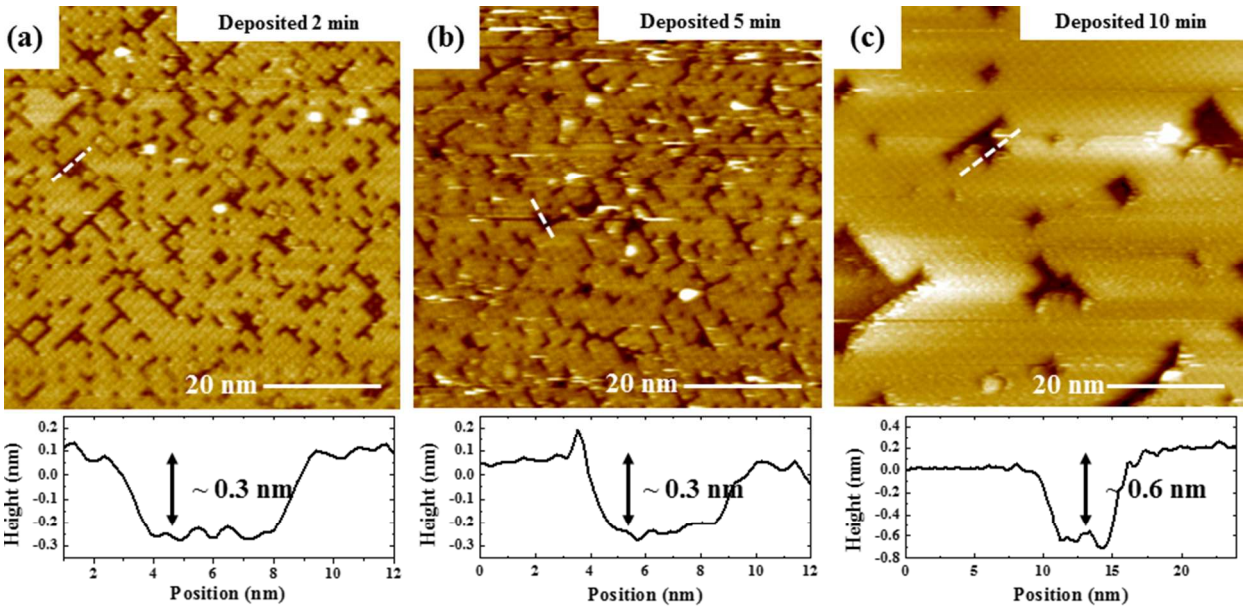

Figure S8. Deposition TiOPc layer on HOPG at 343 K. (Vs = +2.0 V, It = 40 pA). (a) After deposition of TiOPc for 2 min on ML TiOPc at 343 K. (b) After deposition of TiOPc for 5 min on ML TiOPc at 343 K. (c) After deposition of TiOPc for 10 min on ML TiOPc at 343 K.

9. Atomic force microscopy (AFM) image of TiOPc multilayer on HOPG.

To investigate the large area of the 10 nm TiOPc thick film across the multiple HOPG steps, ambient atomic force microscopy (AFM) is performed in the tapping mode, as shown in Fig. S9. Although the growth mode transitions from ML-by-ML to BL-by-BL, molecularly flat TiOPc multilayers are observed by AFM on the HOPG surface after deposition of TiOPc molecules for 10 mins at 373 K. As shown in AFM image of Fig. S9(a), uniform deposition of TiOPc multilayers is observed with large domains. In the expanded AFM image of Fig. S9(b), most of the edges in the top most layer of TiOPc have near identical orientation, as shown by yellow dash lines. It is noted that because of resolution limitation in ambient AFM, some edges of TiOPc layers are not visible as a square. Although some pinholes can be observed in the topmost

layer, these pinholes can be filled by additional deposition of TiOPc. Because of the molecularly flat growth of TiOPc multilayer, the root mean square roughness is only 0.273 – 0.345 nm, consistent with 2 dimensional growth as shown in the line trace of Fig. S9(c). Conversely, other organic molecules mostly grow via layer plus islands or islands growth modes thereby forming truncated pyramidal islands with irregular size consistent with 3D growth and polycrystalline films.[6-7, 9, 13-18]

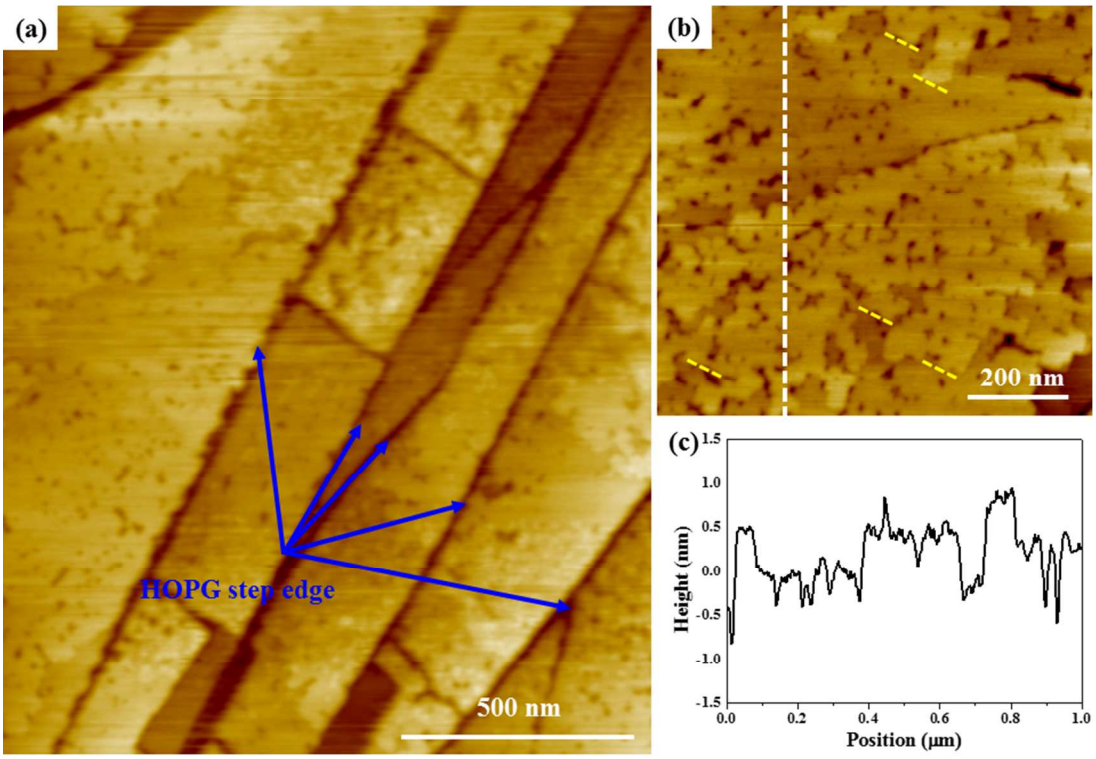

Figure S9. Atomic force microscopy image of TiOPc multilayer (~ 5 nm) deposited on HOPG at 373 K (about 10 nm thickness). (a), Large area AFM image of TiOPc multilayer on HOPG. (b) Expanded AFM image. (c) The line trace profiling of the white dash line of (b).

10. Computational Methods

Density functional theory (DFT) calculations were carried out using the Vienna *ab-initio* Simulation Package (VASP).[19-21] The projector augmented wave method was applied to describe the interactions between valence electrons and frozen cores.[22] An energy cutoff of 400 eV was used. All calculations used spin-polarized DFT. The Perdew−Burke−Ernzerhof (PBE) forms of the generalized gradient approximation (GGA) was used to describe the exchange and correlation interactions.[23] An efficient semi-empirical scheme proposed by Grimme[24] to account for long-range dispersion (van der Waals interactions) corrections was used in all of the calculations. The Gaussian smearing method with a width of 0.1 eV around the Fermi level was applied to facilitate convergence. The electronic energies were converged to 10^{-5} eV. Ionic relaxations were performed until the residual forces on ions were less than 0.02 eV/Å.

The TiOPc-functionalized graphene surface is periodic in the x and y directions, and in z dimension, a minimum vacuum layer of ~10 Å was added to avoid spurious interaction through periodic boundary conditions. The periodic x and y dimensions of supercell were 17.07 × 17.24 $Å^2$. A 1 × 1 × 1 Monkhorst-Pack k-point mesh was chosen to reduce the computational cost. The bonding energy of the TiOPc to the graphene (G) layer was calculated as follows:

$$E_{bind} = E_{tot(n\ TiOPc + G)} - E_{tot(TiOPc)} - E_{tot((n-1)\ TiOPc + G)}$$

where E_{bind} is the bonding energy of n^{th} TiOPc on the surface, $E_{tot(TiOPc)}$ is the total energy of TiOPc in the gas phase, $E_{tot((n-1)\ TiOPc + G)}$ is the total energy of the (n–1) TiOPc functionalized graphene surface, and $E_{tot(n\ TiOPc + G)}$ is the total energy of the n TiOPc adsorbed on graphene surface. Note that bonding energy with a negative value being thermodynamically favorable.

11. Decrease of intermolecular distance of TiOPc films as deposition of multilayer.

As substrate-TiOPc molecule interactions become weaker in TiOPc multilayers, intermolecular interactions dominate the growth of the TiOPc films, resulting in decreased spacing between TiOPc molecules. Fig. S10 displays the center-to-center distance in TiOPc layers versus deposition time of TiOPc ML. Each displayed center-to-center distance is averaged with 60 line traces obtained from five different STM images. As shown in Fig. S8, the ML TiOPc has 1.60 ± 0.02 nm center to center distance, while BL possesses 1.57 ± 0.02 distance, consistent with a reduction of 0.03 nm. As the thickness of TiOPc increases to about 5 nm (total deposition time on ML TiOPc: 5 min), the center-to-center distance in the TiOPc layers decreases additionally to 1.48 ± 0.02 nm. This gradual inverse relation of center-to-center distance versus thickness of the TiOPc film can be explained by the weakened substrate-molecule interactions and enhanced intermolecular interactions.[25-26] In the thin TiOPc film, the substrate-molecule interaction is dominants in the growth of TiOPc; therefore, each TiOPc molecule adsorbs flatly on the TiOPc/HOPG surface. Conversely, in the thick TiOPc film, the substrate-molecular interaction is screened by the pre-deposited TiOPc layer, thereby the intermolecular interaction starts to govern the growth behavior. Therefore, the adjacent molecules in thick TiOPc film layer can be closer laterally than the TiOPc molecules in thin films, because of enhanced intermolecular interaction. It is noted that in most films, this substantial change in lattice constant would induce strain resulting in island growth, but the back-to-back pairs between layer 2 and3, 4 and 5, *etc* ensure the TiOPc have only Van-der-Waals interactions and no steric hindrance to lattice constant changes.

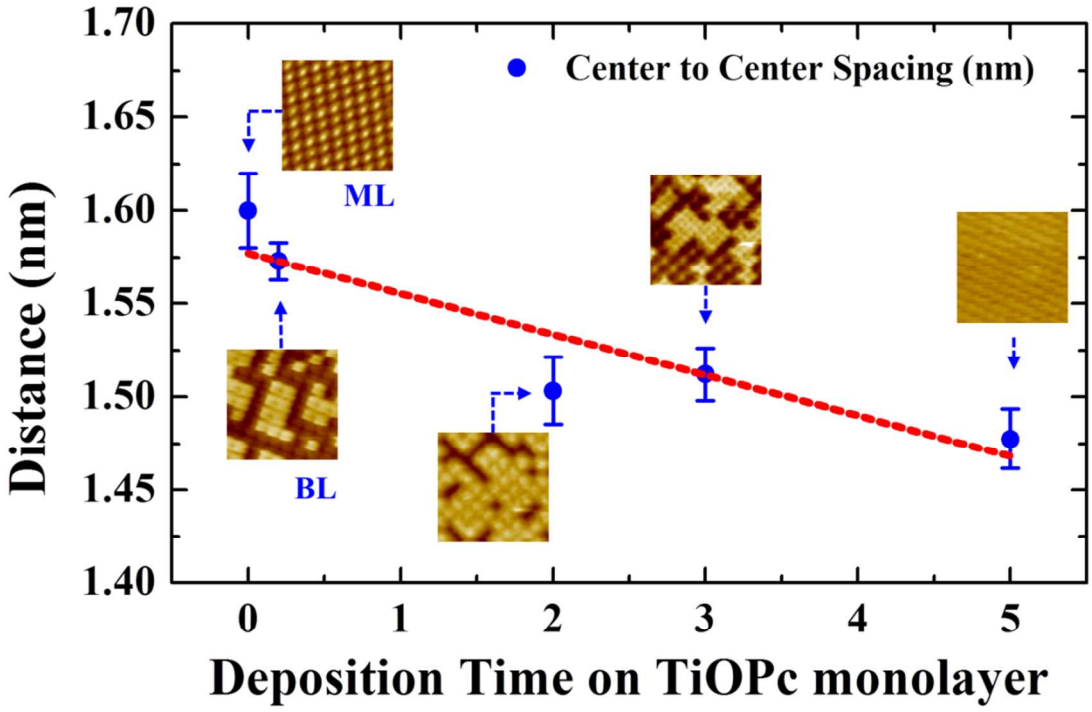

Figure S10. Decreasing center-to-center distance in TiOPc layer with increasing TiOPc layer thickness; linear fit is shown as a red dash line.

12. Vertical intermolecular distance with substrates.

In previous published DFT calculations,[27] FTF pairs in gas phase had shorter intermolecular distance than BTB pairs in gas phase. However, the intermolecular distances in thin layers can be altered by the substrate. As shown in Fig. S11, the intermolecular distances of layers 1, 2, 3 and 4 are calculated with graphene substrates. It is noted that the average distance is calculated from the difference between average z-value of C in graphene and average z-value of C in the respective TiOPc layers. For a single monolayer of TiOPc, TiOPc has a 3.26 Å distance from the graphene substrate. With the adsorption of layer 2, layer 2 has a 3.30 Å distance from the layer 1 after forming a FTF pair, while the distance between the layer 1 and the substrate is constant.

After adsorption of layer 3, a BTB pair is formed between the layer 2 and 3 with a 3.22 Å distance, and the distance between the substrate and layer 1 and the distance between the layer 1 and 2 are slightly decreased. After layer 4 is deposited, another FTF pair is formed between the layer 3 and 4 with a 3.29 Å distance. Comparing this distance of FTF pair to the distance of BTB pair between the layer 1 and 2, the FTF distance between layers 3 and 4 is longer by about 0.1 Å. Consequently, it can be concluded that the intermolecular distance between TiOPc layers are governed by strong interaction with substrates when forming the thin films.

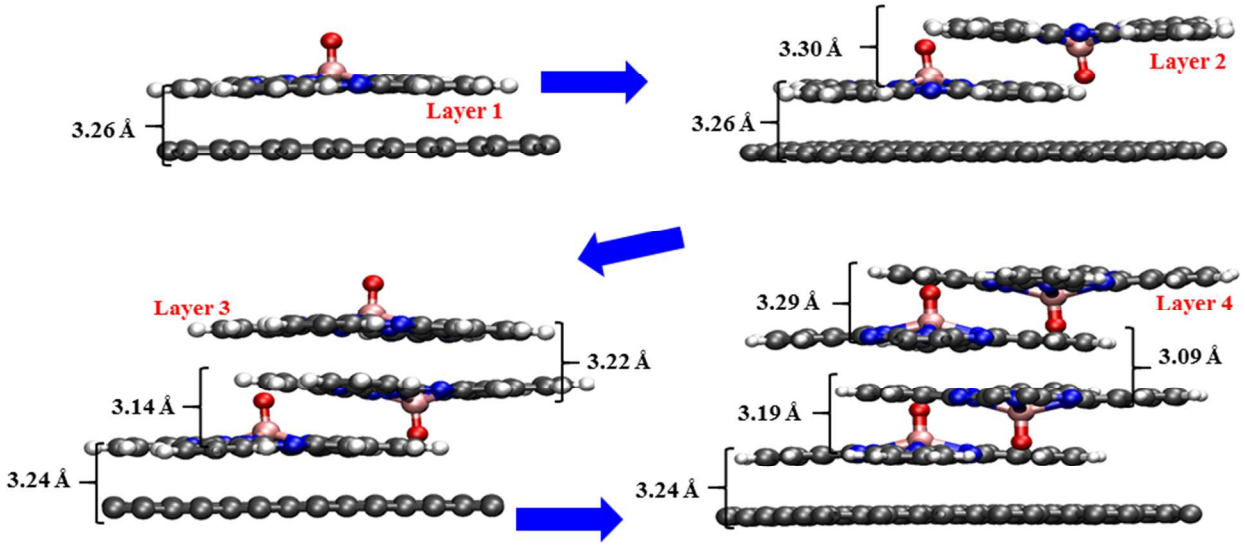

Figure S11. Calculated intermolecular distance between TiOPc layers, with an increase of thickness from monolayer to four layers.

References and Notes

1. Lu X.; Hipps K. W.; Wang X. D.; Mazur U. Scanning Tunneling Microscopy of Metal Phthalocyanines: D(7) and D(9) Cases. *J Am Chem Soc* **1996**, *118*, 7197-7202.

2. Lu X.; Hipps K. W. Scanning Tunneling Microscopy of Metal Phthalocyanines: D(6) and D(8) Cases. *J Phys Chem B* **1997**, *101*, 5391-5396.

3. Takada M.; Tada H. Low Temperature Scanning Tunneling Microscopy of Phthalocyanine Multilayers on Au(111) Surfaces. *Chem Phys Lett* **2004**, *392*, 265-269.

4. Cheng Z. H.; Gao L.; Deng Z. T.; Liu, Q.; Jiang N.; Lin X.; He X. B.; Du S. X.; Gao H. J. Epitaxial Growth of Iron Phthalocyanine at the Initial Stage on Au(111) Surface. *J Phys Chem C* **2007**, *111*, 2656-2660.

5. Wagner S. R.; Lunt R. R.; Zhang P. P. Anisotropic Crystalline Organic Step-Flow Growth on Deactivated Si Surfaces. *Phys Rev Lett* **2013**, *110, (8), 086107*.

6. Stohr M.; Gabriel M.; Moller R. Investigation of the Growth of Ptcda on Cu(110): An Stm Study. *Surf Sci* **2002**, *507*, 330-334.

7. Guaino P.; Carty D.; Hughes G.; McDonald O.; Cafolla A. A. Long-Range Order in a Multilayer Organic Film Templated by a Molecular-Induced Surface Reconstruction: Pentacene on Au(110). *Appl Phys Lett* **2004**, *85*, 2777-2779.

8. Wright J. D. Gas-Adsorption on Phthalocyanines and Its Effects on Electrical-Properties. *Prog Surf Sci* **1989**, *31*, 1-60.

9. Stock T. J. Z.; Nogami J. Copper Phthalocyanine Thin Films on Cu(111): Sub-Monolayer to Multi-Layer. *Surf Sci* **2015**, *637*, 132-139.

10. Nishi T.; Kanai K.; Ouchi Y.; Willis M. R.; Seki K. Evidence for the Atmospheric P-Type Doping of Titanyl Phthalocyanine Thin Film by Oxygen Observed as the Change of Interfacial Electronic Structure. *Chem Phys Lett* **2005**, *414*, 479-482.

11. Krynicki K.; Green C. D.; Sawyer D. W. Pressure and Temperature-Dependence of Self-Diffusion in Water. *Faraday Discuss* **1978**, *66*, 199-208.

12. Lawton E. A. The Thermal Stability of Copper Phthalocyanine. *J Phys Chem-Us* **1958**, *62*, 384-384.

13. Ruiz R.; Choudhary D.; Nickel B.; Toccoli T.; Chang K. C.; Mayer A. C.; Clancy P.; Blakely J. M.; Headrick R. L.; Iannotta S.; Malliaras G. G. Pentacene Thin Film Growth. *Chem Mater* **2004**, *16*, 4497-4508.

14. Gotzen, J.; Kafer, D.; Woll, C.; Witte, G. Growth and Structure of Pentacene Films on Graphite: Weak Adhesion as a Key for Epitaxial Film Growth. *Phys Rev B* **2010**, *81, (8), 085440.*.

15. Gotzen J.; Lukas S.; Birkner A.; Witte, G. Absence of Template Induced Ordering in Organic Multilayers: The Growth of Pentacene on a Cu(221) Vicinal Surface. *Surf Sci* **2011**, *605*, 577-581.

16. Braun D.; Schirmeisen A.; Fuchs H. Molecular Growth and Sub-Molecular Resolution of a Thin Multilayer of Ptcda on Ag(110) Observed by Scanning Tunneling Microscopy. *Surf Sci* **2005**, *575*, 3-11.

17. Gustafsson J. B.; Zhang H. M.; Johansson L. S. O. STM Studies of Thin PTCDA Films on Ag/Si(111)-Root 3x Root 3. *Phys Rev B* **2007**, *75, (15), 155414.*.

18. Huang H.; Chen S.; Gao X. Y.; Chen W.; Wee A. T. S. Structural and Electronic Properties of PTCDA Thin Films on Epitaxial Graphene. *Acs Nano* **2009**, *3*, 3431-3436.

19. Kresse G.; Hafner J. Abinitio Molecular-Dynamics for Liquid-Metals. *Phys Rev B* **1993**, *47*, 558-561.

20. Kresse G.; Furthmuller J. Efficiency of Ab-Initio Total Energy Calculations for Metals and Semiconductors Using a Plane-Wave Basis Set. *Comp Mater Sci* **1996**, *6*, 15-50.

21. Kresse G.; Furthmuller J. Efficient Iterative Schemes for Ab Initio Total-Energy Calculations Using a Plane-Wave Basis Set. *Phys Rev B* **1996**, *54*, 11169-11186.

22. Kresse G.; Joubert D. From Ultrasoft Pseudopotentials to the Projector Augmented-Wave Method. *Phys Rev B* **1999**, *59*, 1758-1775.

23. Perdew J. P.; Burke K.; Ernzerhof, M. Generalized Gradient Approximation Made Simple. *Phys Rev Lett* **1996**, *77*, 3865-3868.

24. Grimme, S. Semiempirical Gga-Type Density Functional Constructed with a Long-Range Dispersion Correction. *J Comput Chem* **2006**, *27*, 1787-1799.

25. Verlaak S.; Steudel S.; Heremans P.; Janssen D.; Deleuze M. S. Nucleation of Organic Semiconductors on Inert Substrates. *Phys Rev B* **2003**, *68, (19), 195409.*.

26. Barrena E.; Palacios-Lidon E.; Munuera C.; Torrelles X.; Ferrer S.; Jonas U.; Salmeron M.; Ocal C. The Role of Intermolecular and Molecule-Substrate Interactions in the Stability of Alkanethiol Nonsaturated Phases on Au(111). *J Am Chem Soc* **2004**, *126*, 385-395.

27. Norton J. E.; Bredas J. L. Theoretical Characterization of Titanyl Phthalocyanine as a P-Type Organic Semiconductor: Short Intermolecular Pi-Pi Interactions Yield Large Electronic Couplings and Hole Transport Bandwidths. *J Chem Phys* **2008**, *128, (3), 034701*.